Wave Synchronizing Crane Control during Water Entry in Offshore Moonpool Operations – Experimental Results

Tor A. Johansen, Thor I. Fossen[1], Svein I. Sagatun, and Finn G. Nielsen[2]

***Abstract*— A new strategy for active control in heavy-lift offshore crane operations is suggested, by introducing a new concept referred to as wave synchronization. Wave synchronization reduces the hydrodynamic forces by minimization of variations in the relative vertical velocity between payload and water using a wave amplitude measurement. Wave synchronization is combined with conventional active heave compensation to obtain accurate control. Experimental results using a scale model of a semi-submerged vessel with a moonpool shows that wave synchronization leads to significant improvements in performance. Depending on the sea state and payload, the results indicate that the reduction in the standard deviation of the wire tension may be up to 50 %.**

I. Introduction

Higher operability of installations offshore of underwater equipment will become increasingly more important in the years to come. Offshore oil and gas fields will be developed with all processing equipment on the seabed and in the production well itself. Norsk Hydro has already one year of operational experience with the Troll Pilot subsea oil processing plant. This subsea plant is made up of a three phase subsea separator, a 1.6 MW electrical single phase pump and a reinjection tree; everything located in 320 m water depth outside the west coast of Norway. The lower cost in using subsea equipment compared to using a floating or fixed production platform is penalized by lower availability for maintenance, repair and replacement of equipment. Production stops due to component failure are costly, hence a high operability on subsea intervention is required to operate subsea fields. High operability implies that subsea intervention must be carried out also during winter time, which in the North Sea and other exposed areas implies underwater intervention in harsh weather conditions.

Standard industrial heave compensation systems applied to offshore cranes or module handling systems (MHS) have been used by the industry for years, see for instance [1], [2], [3], [4], [5] and references therein. These systems normally work with acceleration feedback or feedforward, where the vertical acceleration is measured on the vessel, on the crane boom, or MHS structure. Alternatively, a passive spring-damper mechanism together with position control of the crane hook is used for heave compensation during the water entry phase.

This article focuses on active control of heave compensated cranes or MHS during the *water entry phase* of a subsea installation or intervention. We assume that the payload is launched through a moonpool from a typical mono hull installation vessel. During the water entry phase the hydrodynamic loads due to waves within the moonpool may be significant, and not directly accounted for in a heave compensation system. The main contribution of the present work is the use of moonpool wave amplitude feedforward control in order to achieve wave synchronized motion of the payload through the water entry zone.

Department of Engineering Cybernetics, Norwegian University of Science and Technology, N-7491, Trondheim, Norway. Tor.Arne.Johansen@itk.ntnu.no, tif@itk.ntnu.no

Norsk Hydro Exploration and Production, Bergen, Norway. Svein.Ivar.Sagatun@hydro.com, Finn.Gunnar.Nielsen@hydro.com

II. Mathematical modelling

In this section we describe the dynamics of a laboratory scale model moonpool crane-vessel (scale 1:30). Figures 1 and 2 show a setup consisting of an electric motor and a payload connected by a wire that runs over a pulley suspended in a spring. The spring is designed to simulate a realistic wire elasticity in the scale model. We remark that this setup contains no passive heave compensation system. We will only consider the vertical motion of a payload moving through the water entry zone, handled from the floating vessel. It is assumed that the vessel is kept in a mean fixed position and heading relative to the incoming wave. Effects from the vessel's roll and pitch motion are neglected.

A. Dynamics of scale model crane-vessel

The equations of motion for the motor and payload are

$$m_m \ddot{z}_m = F_m + F_t \quad (1)$$

$$m(\ddot{z} + \ddot{z}_0) = mg + f_z - F_t \quad (2)$$

where $z_m = R\theta_m$, $m_m = J_m/R^2$, $F_m = T_m/R$, and

θ_m	=	motor angle (rad)
R	=	radius of the pulley on the motor shaft (m)
J_m	=	motor inertia (kg/m^2)
T_m	=	motor torque (Nm)
m	=	payload mass (kg)
z_0	=	vessel position in heave (m)
z	=	payload position (m)
z_m	=	motor position (m)
ζ	=	wave amplitude at center of moonpool (m)
F_t	=	wire tension (N)
f_z	=	hydrodynamic and static force on payload (N)

All coordinates and forces are positive downwards. The coordinates z, z_m, ζ_0 and z_p are defined with respect to a vessel-fixed reference frame. The coordinates ζ and z_0 are defined with respect to the Still Water Level, which is fixed with respect to the Earth. The vessel heave position, shown in Figure 2, is fixed in the vessel.

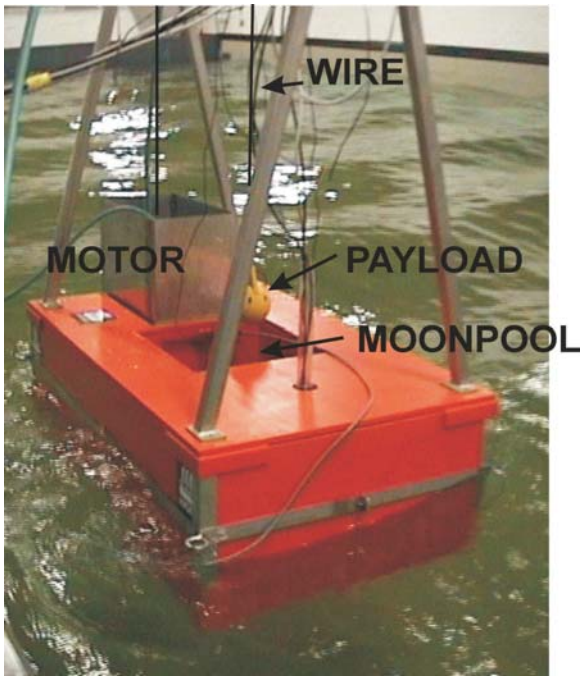

Fig. 1. Vessel-crane scale model.

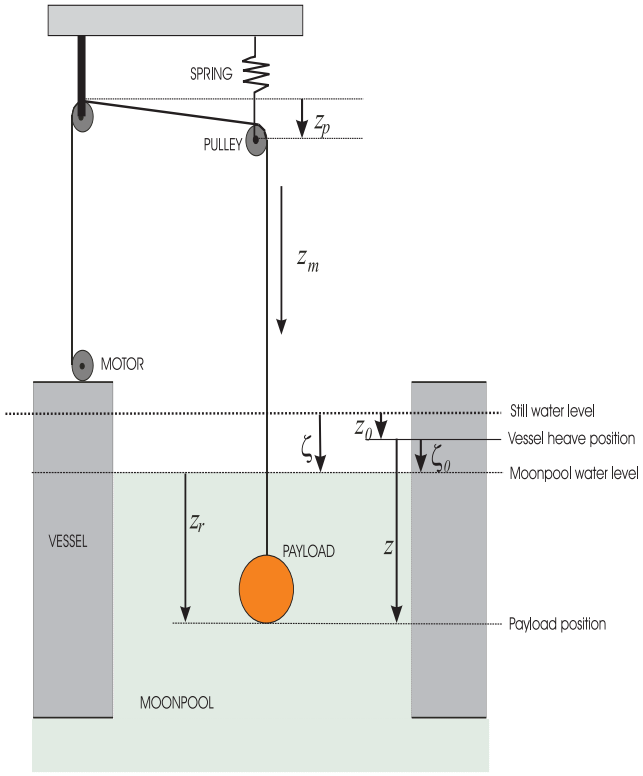

Fig. 2. Definition of coordinates.

The wire runs over a pulley suspended by a spring. The mass moving with the pulley is denoted m_p, and the vertical position of the pulley is z_p. The equation of motion for the pulley is:

$$m_p\ddot{z}_p + d_p\dot{z}_p + k_p z_p = F_t \tag{3}$$

where d_p is the damping coefficient and k_p the spring coeffecient. Substitution of $z = z_m + z_p$ into (3) gives the following expression for the wire force

$$F_t = m_p(\ddot{z} - \ddot{z}_m) + d_p(\dot{z} - \dot{z}_m) + k_p(z - z_m) \tag{4}$$

The hydrodynamic force f_z is given by

$$\begin{aligned} f_z &= -\rho g \nabla(z_r) - \rho \nabla(z_r)\ddot{z} - Z_{\ddot{z}_r}(z_r)\ddot{z}_r \\ &\quad - \frac{\partial Z_{\ddot{z}_r}(z_r)}{\partial z_r}\dot{z}_r^2 - \frac{1}{2}\rho C_D A_{pz}\dot{z}_r\left|\dot{z}_r\right| - d_l\dot{z}_r \end{aligned} \tag{5}$$

see [6], [7], [8], [9], [10]. The symbol ∇ represent buoyancy, $Z_{\ddot{z}_r}$ is position dependence added mass, C_D is the drag coefficient, A_{pz} is the projected effective drag area in the vertical direction, and d_l represents the linear drag. The relative position of moonpool water surface and payload position is z_r, which is assumed to be independent of the horizontal position in the moonpool. The moonpool operates as a piston in a cylinder, such that the water vertical velocity may be assumed to be approximately constant from the wave surface to the bottom of the moonpool. Notice that the impulsive hydrodynamic slamming loads generated when waves hit the product represented by $-\frac{\partial Z_{\ddot{z}_r}}{\partial z_r}(z_r)\dot{z}_r^2$ is directed upward since $\frac{\partial Z_{\ddot{z}_r}}{\partial z_r}(z_r) > 0$.

B. Experimental setup and instrumentation

The total scale model mass is 157 *kg* with a water plane area of 0.63 m^2 and moonpool depth $h_m = 0.29$ m. Further details can be found in [11], [12]. We consider several payloads, including a sphere, a cylinder, and a pump mounted inside an open frame, see Figure 3. The standard payload is a sphere with diameter 0.09 *m* and mass 0.582 *kg*. In full scale, this corresponds to a payload diameter of 2.7 *m* with mass 15.85 tons. The winch motor is an AC servomotor with an internal speed control loop. There are vertical accelerometers in both the payload and vessel, and a wire tension sensor. In the moonpool there are wave meters measuring the wave amplitude in a vessel-fixed coordinate frame, i.e. $\zeta_0 = \zeta - z_0$. The motor position z_m is measured using an encoder.

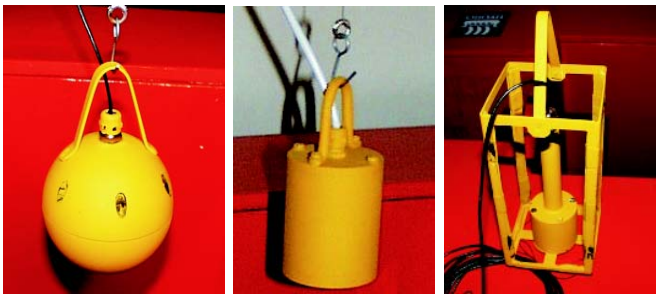

Fig. 3. Payloads used during experiments: sphere, cylinder and offshore pump mounted inside an open frame.

III. Frequency analysis

It can be shown, see [11], that eqs. (1), (2) and (4) lead to the following transfer functions from motor speed to payload

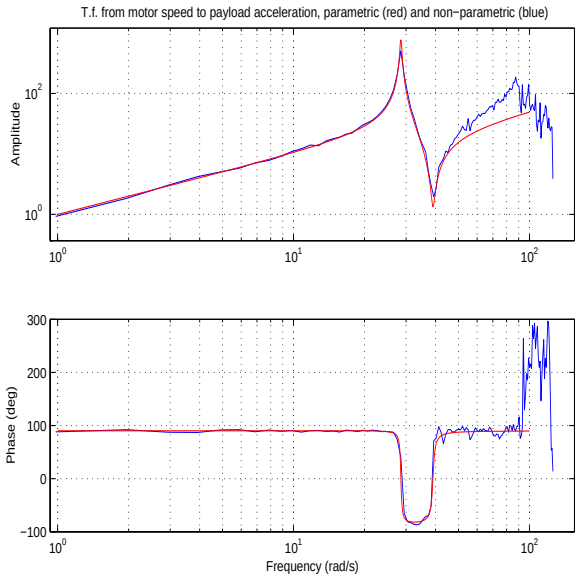

Fig. 4. Parametric and spectral estimates of the transfer function $\ddot{z}/\dot{z}_m(s)$.

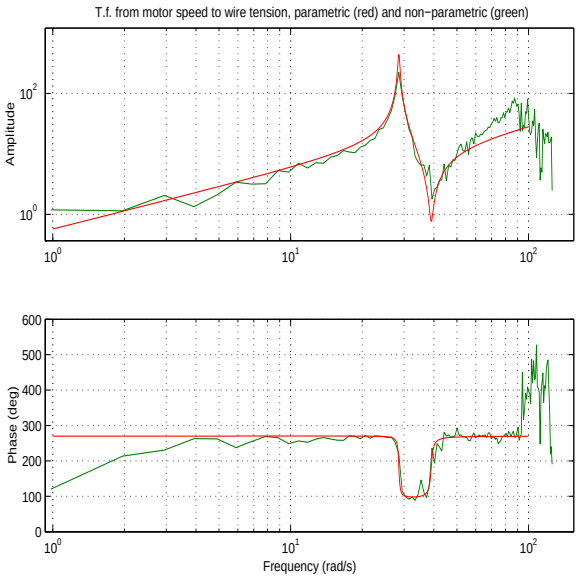

Fig. 5. Parametric and spectral estimates of the transfer function $F_t/\dot{z}_m(s)$.

position and wire tension, respectively, when $f_z = 0$

$$\frac{z}{\dot{z}_m}(s) = \left(\frac{\omega_3}{\omega_2}\right)^2 \frac{1}{s}\left[\frac{s^2+2d_2\omega_2 s+\omega_2^2}{s^2+2d_3\omega_3 s+\omega_3^2}\right] \quad (6)$$

$$\frac{F_t}{\dot{z}_m}(s) = -m\left(\frac{\omega_3}{\omega_2}\right)^2 s\left[\frac{s^2+2d_2\omega_2 s+\omega_2^2}{s^2+2d_3\omega_3 s+\omega_3^2}\right] \quad (7)$$

where s is the complex variable in the Laplace transform, and

$$\omega_1 = \sqrt{k_\delta/m_\delta}, \qquad d_1 = \frac{d_\delta}{2}\frac{1}{\sqrt{m_\delta k_\delta}}$$

$$\omega_2 = \sqrt{\frac{1}{1-m_m/m_\delta}}\omega_1, \qquad d_2 = \left(\frac{\omega_2}{\omega_1}\right)^2 d_1$$

$$\omega_3 = \sqrt{\frac{1}{1+m/m_\delta}}\omega_1, \qquad d_3 = \left(\frac{\omega_3}{\omega_1}\right)^2 d_1$$

satisfying the relationship $\omega_3 < \omega_1 < \omega_2$. The parameters are given by $m_t = m + m_m$, $m_\delta = m_m + m_p(m_t/m)$, $d_\delta = d_p(m_t/m)$, and $k_\delta = k_p(m_t/m)$.

Figure 4 compares spectral and parametric estimates of the transfer function from motor speed to payload acceleration, using the parametric model

$$\frac{\ddot{z}}{\dot{z}_m}(s) = s^2\frac{z}{\dot{z}_m}(s) \quad (8)$$

with the parameters $\omega_2 = 39.0\ rad/s$, $\omega_3 = 28.5\ rad/s$, $d_2 = 0.015\ rad/s$ and $d_3 = 0.008\ rad/s$ for a cylinder shaped payload. The models were identified using experimental data containing several steps in the reference speed, [13], [11]. Likewise, Figure 5 compares the spectral and parametric estimates of the transfer function from motor speed to wire tension, using the parametric model

$$\frac{F_t}{\dot{z}_m}(s) = -m\frac{\ddot{z}}{\dot{z}_m}(s) \quad (9)$$

In these experiments the data were generated while the payload was excited freely in the air. When the payload is partly or fully submerged, the hydrodynamic force f_z given by (5) must be taken into account. This leads to increased damping and effects of added mass and its time-derivative. Depending on parameters such as the size, shape, mass, position and velocity of the payload, a significant reduction in the resonance frequencies (ω_2, ω_3) and increase in the relative damping factors (d_2, d_3) are experienced. $\omega_3 = 48.8$ rad/s is the experimentally determined wire resonance frequency with the spherical payload with mass of 0.572 kg, when the payload is moving in air, [14]. Typical values of ω_3 with the payload in submerged condition are 31 rad/s to 46 rad/s, [14].

The frequency-dependent ratio between wave amplitudes inside the moonpool and in the basin is illustrated in Figure 6. The data are experimental and based on a frequency-sweep using regular waves at 2 cm amplitude. We notice the characteristic resonance near the period $T_m = 1.3$ s, or $\omega_m = 4.83$ rad/s, see also [15]. Typical vessel heave frequencies are in the range $4.0 \leq \omega_{heave} \leq 9.0$ rad/s. The natural frequency of the heave motion of the vessel was found experimentally to be approximately $\omega_{heave} = 4.8$ rad/s, see also [15], [16].

A first order model of the transfer function from the reference speed $\dot{z}_d$ to the motor speed $\dot{z}_m$ is

$$\frac{\dot{z}_m}{\dot{z}_d}(s) = \frac{e^{-0.010s}}{1+0.020s} \quad (10)$$

The time-delay is mainly due to digital communication between the motor drive and control units. At $\omega = 6.3$ rad/s the motor gives a phase loss of approximately 12 deg.

IV. Compensator Strategies

We focus on feed-forward compensator strategies, since the main disturbances can be estimated reliably from measurements, and the wire/suspension elasticity introduces resonances that give fundamental limitations to the achievable feedback control bandwidth. The main performance measures of interest are the wire tension and hydrodynamic forces on the payload. The minimum value must never be less than zero to avoid high snatch loads, and the peak values and variance should be minimized.

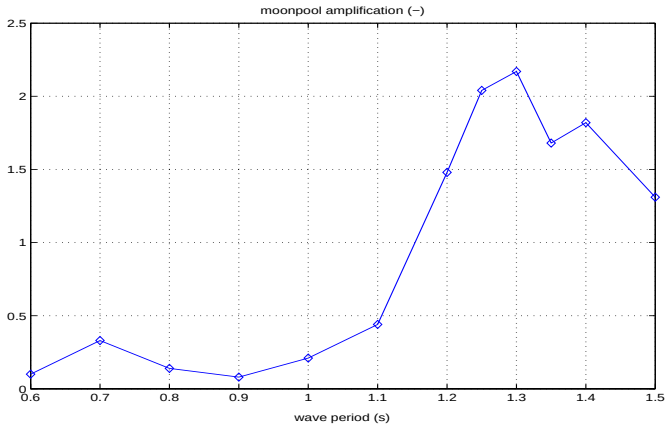

Fig. 6. Ratio between wave amplitudes in moonpool and basin as a function of basin wave period.

A. Active heave compensation

The objective of a heave compensator is to make the payload track a given trajectory in an Earth-fixed vertical reference frame. This means that the payload motion will not be influenced by the heave motion of the vessel. This is implemented using feed-forward where an estimate $\dot{\hat{z}}_0$ of the vessel's vertical velocity (in an Earth-fixed reference frame) is added to the motor speed reference signal $\dot{z}_m^*$ commanded by the operator or a higher level control system:

$$\dot{z}_d \quad = \quad \dot{z}_m^* + \dot{\hat{z}}_0 \tag{11}$$

The vessel vertical velocity $\dot{z}_0$ can be estimated by essentially integrating an accelerometer signal and removing bias using a high-pass filter, because it can be assumed that the vessel oscillates vertically around zero Earth-fixed position (mean sea level):

$$\dot{\hat{z}}_0(s) \quad = \quad \frac{H_{hp}(s)}{s}\ddot{z}_0(s) \tag{12}$$

where $\ddot{z}_0$ is the measured vessel acceleration and $H_{hp}(s)$ is a 2nd order high-pass filter

$$H_{hp}(s) \quad = \quad \frac{s^2}{\omega_c^2 + 2\cdot 0.45\cdot \omega_c s + s^2} \tag{13}$$

with cutoff frequency $\omega_c = 1.37$ rad/s, well below significant wave frequencies.

B. Wave synchronization

Wave amplitude measurements can be used in a feed-forward compensator to ensure that the payload motion is synchronized with the moonpool water motion during the water entry phase. An objective is to minimize variations in the hydrodynamic forces on the payload, $|f_{zd}(z_r)|$, where

$$\begin{aligned} f_{zd} \quad &= \quad -\rho\nabla(z_r)\ddot{z} - Z_{\dot{z}_r}(z_r)\ddot{z}_r - \frac{\partial Z_{\dot{z}_r}(z_r)}{\partial z_r}\dot{z}_r^2 \\ &\quad -\frac{1}{2}\rho C_D A_{pz}\dot{z}_r\left|\dot{z}_r\right| - d_l\dot{z}_r \end{aligned} \tag{14}$$

This equation represents the dynamic part of (5). The first term of (14) is the Froude-Kriloff pressure force. The second term represents the contribution of the added mass, while the third term contains the slamming loads. The last two terms are the viscous and linear drag on the payload. Minimal tension variations are achieved by minimizing variations in $\dot{z}_r$, the relative vertical velocity of the payload and water. This makes intuitive sense, since the linear and viscous drag depend directly on the magnitude of this term, and the Froude-Kriloff pressure depends on $\dot{z}_r^2$. Finally, minimizing high-frequency variations in $\dot{z}_r$ also has a beneficial effect on the added mass since it also leads to reduction in $\ddot{z}_r$. Since $z_r = z - \zeta_0$ we get the approximation $\dot{z}_r \approx \dot{z} - \dot{\zeta}_0\kappa(z)$ by assuming that the wave amplitude decays with depth according to the function $\kappa(z)$. Hence, wave synchronization is achieved by the feed-forward compensator

$$\dot{z}_d \quad = \quad \dot{z}_m^* + \dot{\hat{\zeta}}_0\kappa(z) \tag{15}$$

where $\dot{\hat{\zeta}}_0$ is an estimate of the velocity of the wave surface elevation inside the moonpool (in a vessel-fixed coordinate frame). Since the moonpool operates as a piston in a cylinder, the water vertical velocity may be assumed to be approximately constant from the wave surface to the bottom of the moonpool, and decay exponentially below this point:

$$\kappa(z) \quad = \quad \begin{cases} 1, & z \le h_m \\ \exp(-k(z-h_m)), & z > h_m \end{cases} \tag{16}$$

where h_m is the still water depth of the moonpool with constant circular cross section. Since this control should only be applied during the water entry phase, we introduce the factor $\alpha(z)$ and blends the wave synchronization with heave compensation:

$$\dot{z}_d \quad = \quad \dot{z}_m^* + \dot{\hat{\zeta}}_0\alpha(z)\kappa(z) + \dot{\hat{z}}_0(1-\alpha(z)\kappa(z)) \tag{17}$$

The position-dependent factor $\alpha(z)$ goes smoothly from zero to one when the payload is being submerged, for example

$$\alpha(z) \quad = \quad \begin{cases} 0, & z < 0 \\ z/h_p, & 0 \le z \le h_p \\ 1, & z > h_p \end{cases} \tag{18}$$

where h_p is the height of the payload.

The wave amplitude ζ_0 relative to a vessel-fixed position inside the moonpool is measured. The wave amplitude velocity $\dot{\zeta}_0$ is estimated by filtering and (numerical) differentiation:

$$\dot{\hat{\zeta}}_0(s) \quad = \quad sH_{lp}(s)H_{notch}(s)\zeta_0(s) \tag{19}$$

The low pass filter $H_{lp}(s)$ is composed of a 2nd order critically damped filter at 60 rad/s and a 2nd order critically damped filter at 200 rad/s. In order to avoid exciting the wire resonance, we have introduced a notch filter

$$H_{notch}(s) \quad = \quad \frac{s^2 + 2\cdot 0.1\cdot\omega_n + \omega_n^2}{s^2 + 2\cdot 0.5\cdot\omega_n + \omega_n^2} \tag{20}$$

typically tuned at $\omega_n \approx \omega_3$. In the experiments we used $\omega_n =$ 37 rad/s.

V. Experimental results

In this section we summarize experimental results with the heave compensation and wave synchronization control strategies described above. More data and results with several payloads in regular and irregular waves can be found in [12]. The experiments were carried out in the MCLab at NTNU[1]. The two scenarios we present here represent typical performance improvements that can be achieved:

[1]MCLab - Marine Cybernetcs Laboratory, Trondheim, `http://www.itk.ntnu.no/marinkyb/MCLab/`

- **Spherical payload in regular waves with period $T = 1.25$ s and amplitude $A = 1.8$ cm**. This wave frequency is close to the moonpool resonance frequency, see Figure 6, and the wave amplitude inside the moonpool is about 2 times the basin wave amplitude. The equivalent wave height in full scale is $H_s \approx 1.1$ m.
- **Spherical payload in regular waves with period $T = 1.0$ s and amplitude $A = 6.8$ cm.** At this frequency there is no resonance. The equivalent wave height in full scale is $H_s \approx 4.1$ m.

We present both raw and filtered wire tension data. The filtered data contains mainly components in the frequency band between 3.1 rad/s and 9.4 rad/s, where the significant wave motion is located (the filtering is carried out using 4th order filters with no phase shift). This filtering allows the effects of the wave synchronization to be separated from other effects, since this is the frequency band where the wave synchronization is effective. It is therefore natural to verify the performance of the wave synchronization on the filtered data, neglecting low-frequency components due to buoyancy and high-frequency components due to measurement noise and wire/suspension resonances. Still, it may also be of interest to evaluate the performance of the wave synchronization with respect to excitation of the wire/suspension resonance. This evaluation is, however, not straightforward to carry out since the laboratory model does not contain passive heave compensation or damping. Moreover, the excitations caused by signal noise and winch motor drive are not directly scalable to a full scale implementation and must be considered in the context of the technology used for implementation. Thus, we will base our conclusions mainly on the filtered data.

A. Regular waves at $T = 1.25$ s and $A = 1.8$ cm

Figure 7 shows the payload position and wire tension for test series B (two tests A and B are carried out at each sea state to verify repeatability) with the spherical payload, with and without control. Observations and remarks:

- Wave synchronization in combination with heave compensation reduces the tension standard deviation by 22.0 % in test A and 21.8 % in test B, compared to no control, when considering filtered data.
- The peak minimum tension is changed from 1.21 N to 1.58 N using wave synchronization in test A and from 1.36 N to 1.58 N in test B, compared to no control, when considering filtered data. This is beneficial as it reduces the possibility of wire snatch. The peak maximum tension is somewhat increased with the wave synchronization.
- The use of heave compensation does not give any significant reduction of tension variability in this sea state. However, it gives significant reduction of the standard deviation of the payload acceleration. The reason for this is that the heave motion is fairly small compared to the resonant moonpool water motion.
- When considering the unfiltered data, similar qualitative conclusions can be made.

For the pump-in-frame payload, the wave synchronization in combination with heave compensation reduces the tension standard deviation by 8.9 % in test A and 15.3 % in test B, compared to no control, when considering filtered data.

B. Regular waves at $T = 1.0$ s and $A = 6.8$ cm

Figure 8 shows the payload position and wire tension for test series B with the spherical payload, with and without control. We make the following observations and remarks:

- Wave synchronization in combination with heave compensation reduces the tension standard deviation by 48.1 % in test A and 54.2 % in test B, compared to no control, when considering filtered data.
- The minimum peak tension is changed from 1.36 N to 1.23 N using wave synchronization in test A and from 1.59 N to 1.67 N in test B, compared to no control, when considering filtered data.
- The use of heave compensation alone gives significant reduction of tension variability in this very rough sea state, namely 50.3 % in test A and 25.9 % in test B. This indicates that significant reduction in tension variance can be achieved by either heave compensation or wave synchronization, but largest reduction is achieved by combining them.
- When considering the unfiltered data, similar qualitative conclusions can be made in most cases.

For the pump-in-frame payload the wave synchronization in combination with heave compensation reduces the tension standard deviation by 61.4 % in test A and 53.2 % in test B, when considering filtered data.

C. Discussion

Wave synchronization in combination with heave compensation significantly reduces wire tension variability and peak values in a large majority of the tests. However, under some sea states and for some payloads, no or only small improvement was experienced. The experiments with regular waves showed good repeatability, giving consistent conclusions with different experiments under the same sea state. The position data in Figures 7 and 8 show that wave synchronization utilizes "more control", i.e. more dynamic use of the winch.

Overall, the results are encouraging, showing that wave synchronization has a significant benefit in terms of reduced tension variability and peaks at least under some sea states and with some payloads. Some limitations to performance and sources to uncertainty have been identified:

First, the feed-forward approach leads to a phase error, due to the dynamics of the motor and signal filtering. In our experimental setup this error is significant, and not compensated for. For a wave period of 1.0 s, the phase loss in the motor is 12 deg and the phase loss in the filtering of the wave amplitude measurement is about 25 deg. The total phase loss is around 37 deg. It is therefore reasonable to expect that the use of some model-based short-horizon predictor of the wave amplitude may lead to significant improvement of performance.

Second, the wire/suspension resonance is being excited, also without the use of wave synchronization or heave compensation. The use of these reduces the excitations of the resonance in most cases with the spherical payload, while the excitations of the resonance seems to be typically increased with the pump-in-frame payload. There are several possible sources for these excitations. i) Even with constant speed reference the AC motor drive exhibit oscillations with significant frequency components in area where the resonance frequency is. ii) The water flow inside the moonpool or the heave motion of the vessel may contain frequency components which create hydrodynamic forces that excite the wire resonance. iii) Measurement noise may excite the resonance frequency. Since there is very little damping in the suspension and the resonance frequency is less than a decade above from typical wave frequencies, any filtering will lead to phase loss as described above. A further complication is that the resonance frequency depend on

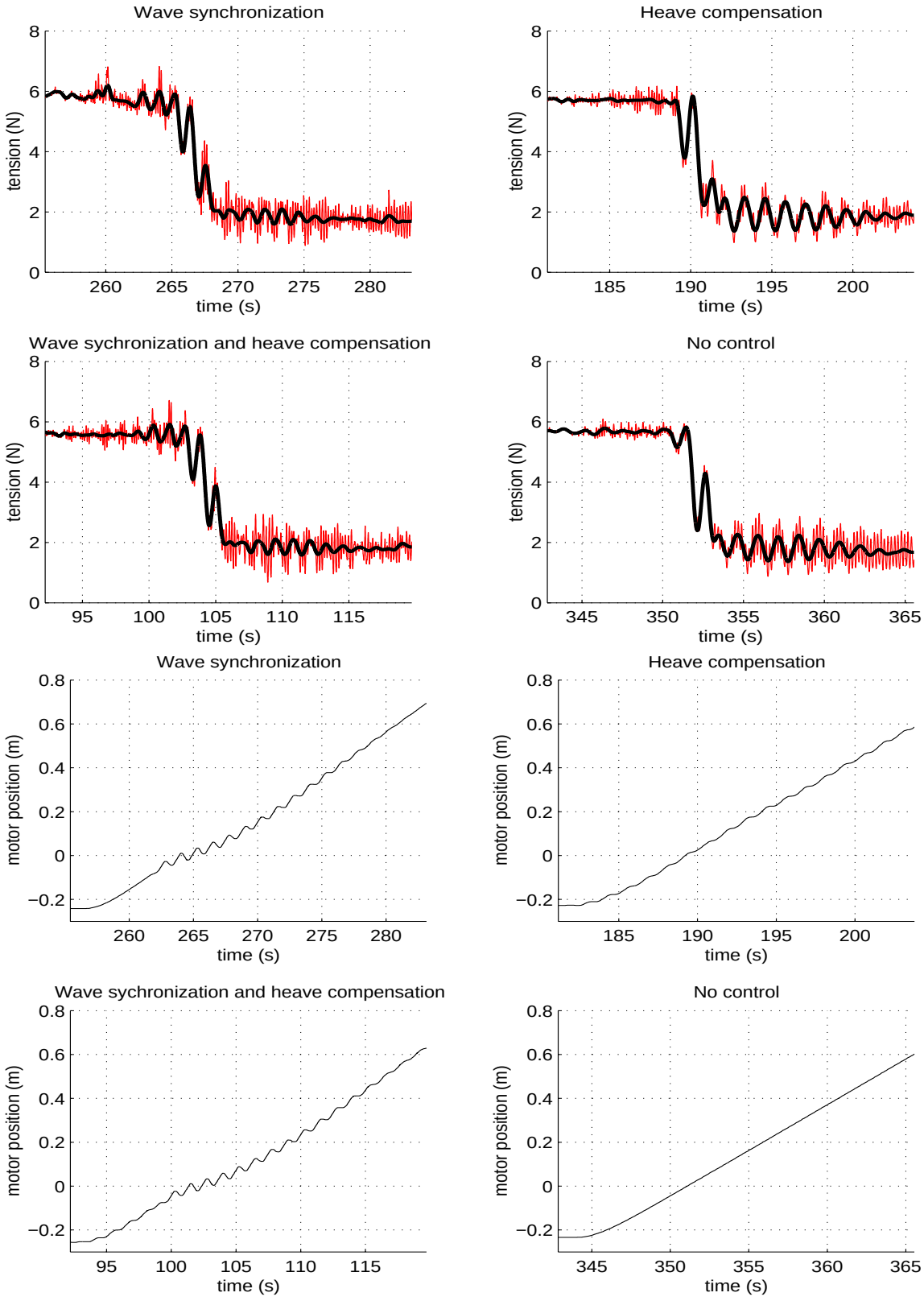

Fig. 7. Experimental results with regular waves at $T = 1.25$ s and $A = 1.8$ cm, spherical payload, test B. For the wire tension we show both raw data (thin lines) and low-pass filtered data (thick lines). The payload position (measured using the motor shaft encoder) is in a vessel-fixed coordinate frame, with zero at mean sea level.

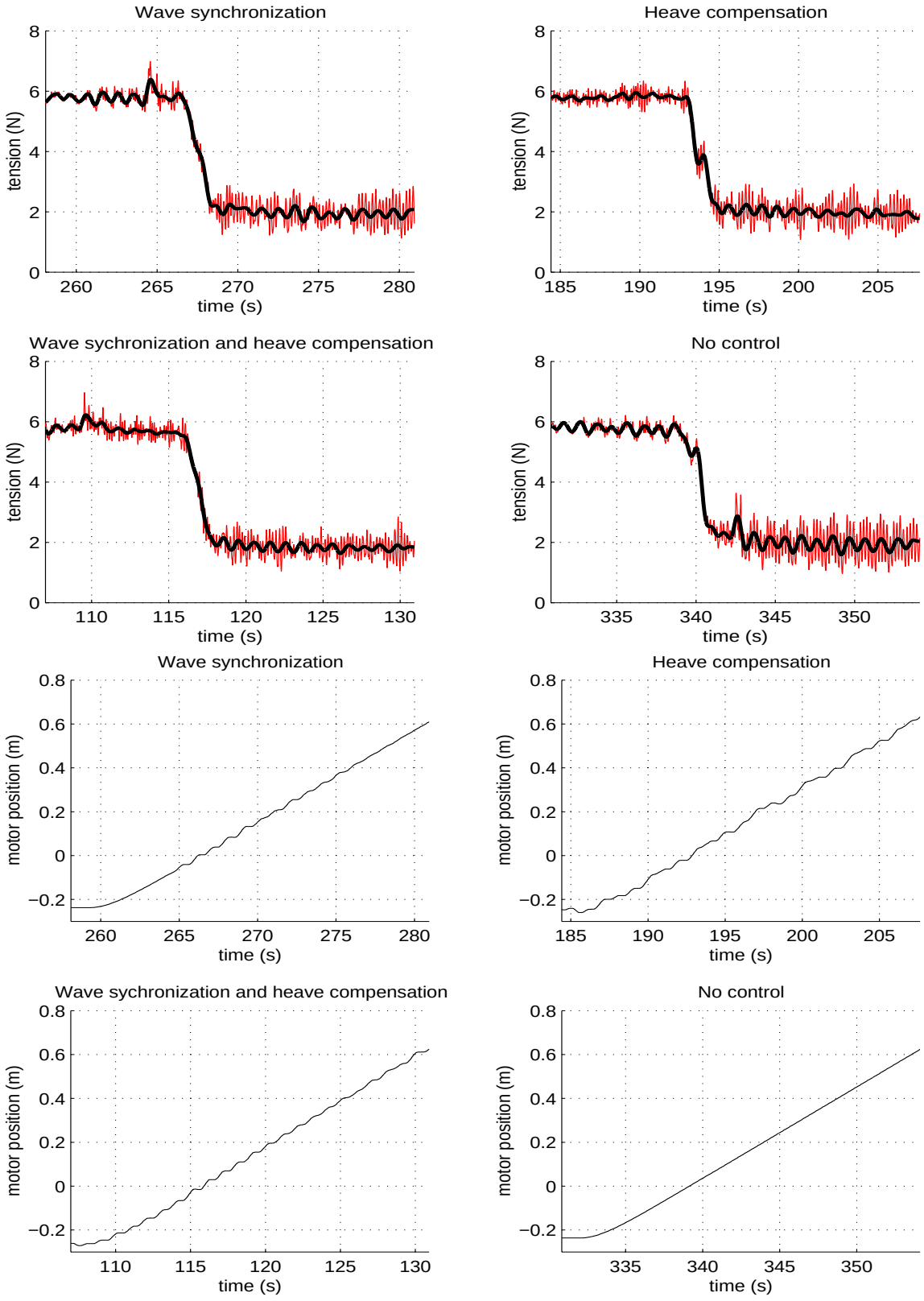

Fig. 8. Experimental results with regular waves at $T = 1.00$ s and $A = 6.8$ cm, spherical payload, test B. For the wire tension we show both raw data (thin lines) and low-pass filtered data (thick lines). The payload position (measured using the motor shaft encoder) is in a vessel-fixed coordinate frame, with zero at mean sea level.

payload mass and position-dependent hydrodynamic properties such as added mass. Improvements may be expected by adaptive notch filtering, in combination with wave prediction to account for the phase loss. Obviously, the technical solutions for wave measurements, signal transmission and electronics may be modified to reduce the overall noise level. Noise is amplified due to numerical differentiation when computing the wave surface speed from the wave amplitude measurements, and alternative methods to measuring the relative velocity of the water and payload are of interest.

D. Scaling considerations

The experiments are scaled with respect to the Froude number, a dimensionless number defined as the fraction between the inertial and gravitational forces $\mathrm{Fr} = \dot{z}/\sqrt{gr}$ where r is a characteristic radius. Thus, all elastic effects are well accounted for as long as the frequencies are properly scaled. Frequency in the model scale f_m is scaled with $\lambda^{\frac{1}{2}}$, that is $f = \lambda^{-\frac{1}{2}} f_m$ where $\lambda = 30$ is the scale factor used in the experiments. Viscous effects are normally scaled with respect to the Reynolds number . The Reynolds number is dimensionless variable which represents the fraction between inertia and viscous effects defined as follows: $\mathrm{Re} = \dot{\zeta} r/\nu$ where ν is kinematic viscosity. The relationship between full scale and the model scale Reynolds numbers when using Froude scale becomes $\mathrm{Re} = \lambda^{\frac{3}{2}} \mathrm{Re}_m$ where the subscript m denotes model scale. A typical Reynolds number in the experiments is $5 \cdot 10^4$ while the Reynolds number in the full scale case normally is in the range of 10^6. This discrepancy in Reynolds number may have an effect for streamlined bodies, like the sphere, but may most likely be neglected for bluff bodies since the separation point (of vortices) becomes the same for scaled and full scale bluff bodies. Damping is normally over predicted in model scale experiments due to viscous effects. This causes an under prediction of the response which is important to take into account when transferring the experimental data to full scale. The effects from elasticity are well taken care of in the model scale since all frequencies are scaled correctly.

VI. Conclusions

It is shown via scale model experiments that the performance of offshore moonpool crane operations can be significantly improved by wave synchronization in combination with heave compensation. This can be implemented as a feedforward compensator within an active heave compensation system, using measurement of the wave amplitude in the moonpool.

Acknowledgements

The authors are grateful to Marintek for kind assistance during the experiments.

References

[1] NSLT, *The 5th North Sea Offshore Crane Conference, Aberdeen, Scotland*. Norwegian Society of Lifting Technology (NSLT), 2000.

[2] ——, *Underwater Lifting Operations, Stavanger, Norway (in Norwegian)*. Norwegian Society of Lifting Technology (NSLT), 2000.

[3] ——, *The 3th International Offshore Crane Conference, Kristiansand, Norway*. Norwegian Society of Lifting Technology (NSLT), 1998.

[4] S. I. Sagatun, T. I. Fossen, and K. P. Lindegaard, "Inertance control of underwater installations," in *Preprint IFAC CAMS, Glasgow, Scotland*, 2001.

[5] U. A. Korde, "Active heave compensation on drill-ships in irregular waves," *Ocean Engineering*, vol. 25, pp. 541–561, 1998.

[6] S. I. Sagatun, T. A. Johansen, T. I. Fossen, and F. G. Nielsen, "Wave synchronizating crane control during water entry in offshore moonpool operations," in *Proc. IEEE Conf. Control Applications, Glasgow*, 2002.

[7] O. M. Faltinsen, *Sea Loads on Ships and Offshore Structures*. Cambridge University Press, New York, 1990.

[8] J. N. Newman, *Marine Hydrodynamics*. Cambridge, MA: MIT Press, 1977.

[9] M. Greenhow and L. Yanbao, "Added masses for circular cylinders near or penetrating fluid boundaries - review, extension and application to water-entry, -exit and slamming," *J. Ocean Engineering*, vol. 14, pp. 325–348, 1987.

[10] S. I. Sagatun, "Active control of underwater installation," *IEEE Trans. Control Systems Technology*, vol. 10, pp. 743–749, 2002.

[11] T. I. Fossen and T. A. Johansen, "Modelling and identification of offshore crane-rig system," Department of Engineering Cybernetics, NTNU, Trondheim, Norway, Tech. Rep. 2001-12-T, http://www.itk.ntnu.no/research/HydroLab/reports/-hydrolaunch_model.pdf, 2001.

[12] T. A. Johansen and T. I. Fossen, "Observer and controller design for an offshore crane moonpool system," Department of Engineering Cybernetics, NTNU, Trondheim, Norway, Tech. Rep. 2001-13-T, http://www.itk.ntnu.no/research/HydroLab/reports/-hydrolaunch_control.pdf, 2001.

[13] T. Söderström and P. Stoica, *System Identification*. Prentice Hall, Englewood Cliffs, NJ, 1988.

[14] T. A. Johansen and T. I. Fossen, "HydroLaunch free decay tests," Department of Engineering Cybernetics, NTNU, Trondheim, Norway, Tech. Rep. 2001-18-T, http://www.itk.ntnu.no/research/HydroLab/-reports/hydrolaunch_free_decay.pdf, 2001.

[15] F. G. Nielsen, "Coupled hydrodynamics for the HydroLaunch vessel with load," 2002, working note, Norsk Hydro, Exploration and Production, Bergen, Norway, http://www.itk.ntnu.no/research/HydroLab/-reports/HydroLab_dynamics.pdf.

[16] M. P. Fard and F. G. Nielsen, "Simulation of coupled vessel-load dynamics," Norsk Hydro, Exploration and Production, Bergen, Norway, Tech. Rep. NH-00036960, http://www.itk.ntnu.no/research/HydroLab/-reports/Fard2002.pdf, 2001.